INTERNAL REPORT #79

THE AUGUST, 1976 ELECTRON

CALIBRATION OF TET

by

J. Zmuidzinas

N. Gehrels

Space Radiation Laboratory

California Institute of Technology

Pasadena, California

3-3-81

Abstract.   This report is about the electron calibration of The Electron Telescope (TET) which is part of the Cosmic Ray Subsystem onboard Voyagers 1 and 2. The calibration was performed at the Intelcom Rad Tech Linac in La Jolla during August, 1976. The report contains a summary of the accelerator run itself, including the setup and the problems encountered, a description of the analysis technique and the methods by which the problems were solved, and the resulting isotropic electron energy response curves for the TET ranges.

I. Introduction

The Electron Telescope (TET) is a lightweight (0.6 kg) electron energy spectrometer that is part of the Cosmic Ray Subsystem onboard the Voyager spacecraft. Its design and science objectives are described in Stone et al, [1977] and Whitcomb, [1973]. TET consists of eight grooved silicon solid state detectors (D1-D8) and six tungsten absorbers (A1-A6) in a cylindrical geometry (see Figure 1). The detectors have outside rings which are used as anticoincidence guards. To identify electrons and measure their energies, TET uses a double dE/dx measurement in D1 and D2 and a range measurement as determined by the penetration into detectors D3 to D7.

TET has an energy range of approximately 5 MeV to 110 MeV. There are two effects which make it very hard to calculate the telescope's response to electrons of these energies:

1) This energy range brackets the electron critical energy in tungsten - the energy at which radiation energy loss and ionization energy loss become equally important (~8.1 Mev in tungsten). Therefore, any calculation would have to include both processes. Furthermore, since the radiated photons can pair-produce, any calculation or program would have to follow a multitude of electrons, positrons, and photons in order to be accurate.

2) Collisions with silicon or tungsten atoms can result in large angle scatterings. Thus, electrons near the end of their range can suddenly scatter into a guard ring, nullifying the event. Also, electrons with an incident direction nearly perpendicular to the axis of the telescope can undergo a large angle collision and scatter into the telescope. Thus the effective geometry factor is not necessarily the one defined by the areas of two separated overlapping disks.

It was therefore necessary to calibrate TET experimentally. This calibration was performed at the Intelcom Radtech Linac electron accelerator in La Jolla, California during August, 1976 using the calibration telescope. The rest of this report is devoted to the description of the accelerator run and the analysis of the data.

II. Description of Accelerator Run

In this section the equipment setup and the problems encountered at the La Jolla accelerator calibration will be briefly described. More information can be found in the calibration notebook, the picture notebook, the computer printout binder, and the RPC (Rick's proportional counter) handbook, all in Room 207 (or see A. Cummings).

A diagram of the equipment arrangement is shown in Figure 2. The equipment was aligned with respect to the beam pipe using a "T" placed on the frame of the 1 mil Ti window at the end of the pipe. A copper scattering foil was placed ~2 cm in front of the Ti window to widen the profile of the beam. The objective was to create as uniform a flux as possible on TET while still maintaining a narrow enough beam to keep most of the electrons within the multiwire proportional counter (PC) area. The foil thickness that was used ranged from 0 to 15 mils (Cu) and is listed for each run in the calibration notebook.

Next in line toward TET was a bag made out of $\sim\frac{1}{4}$ mil aluminized mylar supported by a wooden frame, and filled with helium. For the 6-21 MeV runs (the energies chosen for the runs will be discussed later) a 20 cm long bag was used, and for the 28-85 MeV runs the bag length was 80 cm. The purpose of the He was to reduce the probability of a scattering or bremsstrahlung interaction in the region near TET.

Immediately in front of TET was the PC. A description of the PC and its signal input into PACE is given in Appendix A. The purpose of the counter was to determine the vertical and lateral position of each electron and to allow a separation of single and multiple electron events. The position information is used to calculate the absolute flux incident on TET and correct for its nonuniformity as described in section V of this report. The multiple electron rejection technique is described in section IV.

The PC, cathode preamps, anode discriminator boxes and TET junction box and preamps were all mounted on a $\sim\frac{1}{4}$" thick aluminum base plate. TET was attached to an aluminum pole protruding through a hole in the plate and mounted on a rotation table below, allowing remote

rotation of the telescope axis with respect to the PC and the electron beam. The axis of symmetry of the telescope was ~6" above the plate. Calibration measurements showed that the angle between a side of the pole holding TET and an alignment line on the base plate could be reproduced remotely to within ~1°.

The eight detectors (D1,D2,...D8) and the eight guard rings in TET were connected to preamps through a junction box where G1, G3, G5 and G7 and G2, G4, G6, and G8 were combined to form GA and GB, respectively. Each signal D1,...D8, GA and GB (as well as X1, X2, Y1, Y2 from the PC) went into a TC164 preamp mounted on the base plate and then a TC213 postamp in a nearby rack. Fifty foot coaxial cables connected the postamps to PACE channels and the PC anode discriminators to the external word input box. The format of the PACE event words is given in Appendix B. A pulser calibration of the amplifier gains was performed and listings of energy loss vs. PACE channel number made (see calibration notebook) before and after the accelerator run.

The entire calibration lasted four days. The beam energies that were used are, in chronological order, 28, 39, 53, 72, 85, 6, 8, 11, 15 and 21 MeV. The original plan had been to calibrate up to 100 MeV, but the Linac was not operating over 85 MeV while we were there. Even the 85 MeV run was of questionable quality for two reasons:

1) The beam was broader than expected, indicating that the electrons were being scattered prior to exitting the beam pipe. This was a bad sign since it implied an unknown amount of beam contamination (photons, positrons, and lower energy electrons).

2) The beam energy drifted down from 88 to 85 MeV during the run and was very irregular in intensity.

For these reasons, the 85 MeV run is not included in the analysis below.

For the 39 to 85 MeV runs, the Linac RF signal induced a large enough noise level in the guards during beam dumps to trigger the PACE discriminator thresholds. Since the discriminators were set at the correct spacecraft levels (200 keV for GA and GB), there was reluctance to raise them. However, for the 72 and 85 MeV runs, the GB signal became so noisy

that PACE was being triggered by it every beam dump. The threshold level was therefore increased to ~330 keV; the GA threshold was similarly increased for the 85 MeV run. The way in which the noise events and the change in threshold are dealt with in the analysis of the data is described in section VI.

During the 53 and 72 MeV runs an intermittent hardware problem (the infamous "double image" problem) occurred that affected the PC signals. The symptom was a double image of TET in the vertical direction of the PC. The cause was never fully determined although it appeared to be correlated to certain cable - PACE stretcher combinations. The runs that were affected were not used in the analysis of the data.

The final problem, that was only discovered after the calibration run, was that the discriminator threshold (PACE LLD) on D8 had been set at 500 keV instead of the spacecraft level of 200 keV. The problem was easily remedied in the analysis by using the D8 pulse height information, recorded by PACE even if a given channel is not triggered, to determine which events would have had a D8 tag if the discriminator had been set at 200 keV.

III. Method Used To Measure Response

Assuming an isotropic incident electron flux, the counting rate in each TET range ($D1D2\cdots DN\overline{DN+1}\overline{DN+2}...\overline{GA}\overline{GB}$, abbreviated D_{1-N}) is given by

$$(1) \qquad D_{1-N} = A\Omega_{1-N} \int_0^\infty \frac{dJ}{dE}(E)\ R_{1-N}(E)\ dE$$

where $A\Omega_{1-N}$ is the physical geometry factor (cm^2-sr) of the two disks D1 and DN (listed in Table 1), $\frac{dJ}{dE}(E)$ is the electron spectrum (e/cm^2-sr-MeV-sec) and $R_{1-N}(E)$ is the omni-directional detection efficiency for range N as a function of energy (a dimensonless "response function"). Thus, if we know the response functions, we can unfold the spectrum from the counting rates. The purpose of the accelerator calibration was to measure the response functions. Note that the only restrictions we have put on the events are that they be range N events with no guard tags. However, when trying to minimize the proton background, additional requirements such as upper limits for D1 and D2 pulse heights and upper thresholds for D3-D7 can be used (see e.g., Whitcomb, 1973). The flight electronics imposes an absolute upper limit of 2.5 MeV on the D1 and D2 pulse heights, but this limit can be lowered when analyzing the flight data by using the pulse height information. Whenever a new limit is used or any new requirement is imposed, new response curves must be generated with the same conditions applied to the accelerator data.

The accelerator produces a beam of electrons rather than an isotropic flux. The count rate from a non-isotropic flux is given by

$$(2) \qquad D_{1-N} = A\Omega_{1-N} \int_0^\infty \int_0^\pi \int_0^{2\pi} \frac{dJ}{dE}(E,\vartheta,\varphi)\ \tau_{1-N}(E,\vartheta,\varphi)\ d\varphi\ \sin(\vartheta)\ d\vartheta\ dE$$

where ϑ and φ are the polar angles relative to the axis of the telescope, $\frac{dJ}{dE}(E,\vartheta,\varphi)$ is the non-isotropic electron spectrum, and $\tau_{1-N}(E,\vartheta,\varphi)$ is the detection efficiency as a function of energy and angle. Assuming the beam has a uniform cross section and a narrow spread in both energy and angle, we can write

$$\frac{dJ}{dE}(E,\vartheta,\varphi) \;=\; J_0\,\delta(E-E_0)\,\frac{\delta(\vartheta-\vartheta_0)\,\delta(\varphi-\varphi_0)}{\sin(\vartheta)}$$

where E_0 is the incident electron energy, ϑ_0, φ_0 describe the direction of the beam, and J_0 is the incident flux (e/cm^2-sec). From equation 2, the count rate in each range as a function of angle at the accelerator, $A_{1-N}(E_0,\vartheta_0,\varphi_0)$, is given by

$$A_{1-N}(E_0,\vartheta_0,\varphi_0) \;=\; A\Omega_{1-N}\,J_0\,\tau_{1-N}(E_0,\vartheta_0,\varphi_0)\;.$$

Since TET has a cylindrical geometry, $\tau_{1-N}(E_0,\vartheta_0,\varphi_0)$ is independent of the azimuthal angle φ_0, and we can thus write

$$(3)\qquad \tau_{1-N}(E_0,\vartheta_0) \;=\; \frac{A_{1-N}(E_0,\vartheta_0)}{A\Omega_{1-N}\,J_0}\;.$$

At the Linac in La Jolla, A_{1-N} and J_0 were measured for various energies and angles (10 energies and about 8 angles per energy). J_0 was measured using the proportional counter in front of TET. Since the same time interval is used to measure both the rate and the flux,

$$(4)\qquad \tau_{1-N}(E_0,\vartheta_0) \;=\; \frac{1}{A\Omega_{1-N}}\,\frac{\#\ \text{of range N events}}{\#\ \text{events per unit area}}\;.$$

In order to relate the angular response function $r_{1-N}(E,\vartheta)$ to the isotropic response function $R_{1-N}(E)$, an isotropic flux, $\frac{dJ}{dE}(E,\vartheta,\varphi) = \frac{dJ}{dE}(E)$, is substituted into (2) to give

$$D_{1-N} = A\Omega_{1-N} \int_0^\infty \int_0^\pi \int_0^{2\pi} \frac{dJ}{dE}(E)\, r_{1-N}(E,\vartheta)\, d\varphi\, \sin(\vartheta)d\vartheta\, dE$$

$$= A\Omega_{1-N} \int_0^\infty \frac{dJ}{dE}(E)\, 2\pi \int_0^\pi r_{1-N}(E,\vartheta)\, \sin(\vartheta)d\vartheta\, dE \ .$$

Comparison with equation (1) gives

$$(5) \qquad R_{1-N}(E) = 2\pi \int_0^\pi r_{1-N}(E,\vartheta)\, \sin(\vartheta)d\vartheta \ .$$

This expression can be numerically integrated using the measured values of r_{1-N} (equation 4).

Note that we divide by the geometry factor $A\Omega_{1-N}$ in equation 4 to obtain the response function, and multiply by the same factor when using the response function in equation 1. $A\Omega_{1-N}$ is therefore only a normalizing factor used in the definition of $R_{1-N}(E)$ to give it the physical meaning of $\frac{A\Omega_{effective}}{A\Omega_{1-N}}(E)$. At the accelerator we measure the effective geometry factors of TET's various ranges as a function of energy.

IV. Multiple Electron Event Rejection

The Linac produces particles in bursts or "dumps" of ~1 μs duration at a rate set at ~460 dumps/sec for the calibration. By changing the beam intensity the operators could adjust the average number of particles per dump to our specifications. Since PACE typically has a resolving time of 2-3 μs, all of the particles in a dump are recorded as a single event. Therefore, the objective was to choose an intensity that would give a small fraction of multi-electron dumps relative to one-electron dumps and yet give a reasonable rate of one electron dumps. The distribution of particles per dump is theoretically a Poisson distribution, so that by choosing an average rate of 0.5 particles per dump (an extremely low rate for this Linac) we obtained approximately 61% of the dumps with 0 electrons, 30% with 1 electron, 8% with two electrons, etc. This section deals with techniques used to separate the double (or more) electron events from the single electron events.

There are two independent checks that can be used to separate the doubles from the singles, both of which involve using the proportional counter in front of TET. For more details on the PC , see Appendix A. The first check uses the anode wires of the PC. (In this report, the term "anode wire" refers to a group of three adjacent wires that are tied together as described in Appendix A.) We shall label events according to the number of anode wires fired in each direction. For example, a (1,2) event fired one anode wire in the x direction and two anode wires in the y direction. The check throws out all events that fire more than one anode wire in either direction (i.e. only (1,1) events are kept). Double electron events in which the two electrons hit different sections of the PC will be thrown out. However, double events in which the two electrons are close enough to each other to fire the same anode wires can get by this test. (There are 8 anode wires in each direction; therefore, about 1 out of 64 of the double electron events in a uniform beam will fire the same anode wires in both directions.) Also, single electron events that fall exactly in between two wires will fire both, so some singles will be thrown out. Great care must be used when throwing these events out, as they

lie on a grid pattern. Since this nonuniform rejection could bias the response calculation, one must make sure that the number of singles thrown out is very small.

The second check uses the average of the four cathode pulse heights as a measure of ionization energy loss. Single minimum ionizing electrons lose roughly 2 MeV-cm^2/g (ionization energy loss only; Rossi p. 25 [1952]), or approximately 4 KeV per cathode plane in the PC. Two electrons will lose twice as much, on the average. The check separates double electron events from single electron events by throwing out events that have an average cathode pulse height (a.c. pht.) above a predetermined cutoff called the s/d (singles/doubles) cutoff. A plot of the a.c. pht. distribution (Figure 3c) shows clear single and double electron peaks which can be separated approximately using the anode check. Figures 3b and 3a show the a.c. pht. distributions for single anode wire events ((1,1) events ; mostly single electron events) and for events having two anode wires in each direction ((2,2) events ; nearly all doubles), respectively. With the cutoff set below a good portion of the doubles peak, doubles that slip past the anode check will have a high probability of being thrown out with this check (assuming (1,1) doubles have the same a.c. pht. distribution as (2,2) events; see below). Care must be taken, however, to make the cutoff high enough so that the number of singles lost is not too great.

We would like to estimate the fraction of single electron events lost and the fraction of double electron events kept by these two checks.. To do this, we estimate these numbers separately for each check. For the cathode check, these numbers are determined using the a.c. pht. distributions. The (1,1) distribution (Figure 3b) is assumed to consist entirely of singles, so the fraction of single electron events lost is the ratio of the number of events in this distribution that are above the cutoff to the total number of events in the distribution. Similarly, the (2,2) distribution (Figure 3a) is assumed to consist entirely of doubles, so the fraction of doubles kept is the ratio of the number of events in this distribution that are below the cutoff to the total number of events in the distribution. It is also assumed in this calculation that the a.c. pht. distribution for (1,1) double electron events is the same as the

(2,2) distribution. This is a reasonable assumption since the energy lost in the proportional counter by the second electron should be independent of where that electron hits. We can write the formulas for these ratios symbolically :

(6)
$$\begin{array}{l} \text{\% singles lost} \\ \text{due to cathode} \\ \text{analysis} \end{array} = \frac{\text{\# (1,1) events} > \text{s/d cutoff}}{\text{\# (1,1) events}} \times 100$$

(7)
$$\begin{array}{l} \text{\% doubles kept} \\ \text{by cathode} \\ \text{analysis} \end{array} = \frac{\text{\# (2,2) events} \leq \text{s/d cutoff}}{\text{\# (2,2) events}} \times 100$$

These ratios are plotted for various choices of the s/d cutoff in Figure 4 using 28 MeV 0 Deg. data. The s/d cutoff in this case was chosen to be 3000.

It is somewhat more difficult to calculate these numbers for the anode analysis. To calculate the fraction of singles thrown out, we look only at events whose a.c. pht. is small. This insures that they are single electron events. The fraction is calculated by

(8)
$$\begin{array}{l} \text{\% singles lost} \\ \text{due to anode} \\ \text{analysis} \end{array} = \frac{\text{\# multiple anode events} \leq \text{small a.c. pht.}}{\text{\# (1,1) events} \leq \text{small a.c. pht.}} \times 100 \quad .$$

The doubles kept ratio uses (1,1) events that have a large a.c. pht. to insure that they are mainly doubles. However, there are other doubles that have lower a.c. pht.'s. To take these into account we use the relation

$$\text{\# (1,1) events} > \text{large acp} = \text{\# (1,1) doubles} \times \text{Prob. double} > \text{large acp} \quad .$$

By inverting this formula, we can calculate the number of (1,1) doubles. However, we need the probability that a double will have an a.c. pht. larger than the chosen large a.c. pht. limit (large acp). For this, we use the (2,2) a.c. pht. distribution. The probability, P, is given by

$$P = \frac{\text{\# (2,2) events} > \text{large acp}}{\text{\# (2,2) events total}}$$

so

$$\text{\# (1,1) doubles} = \frac{\text{\# (1,1) events} > \text{large acp}}{P} \quad .$$

The fraction of doubles kept is the ratio of this number to the total number of doubles (approximately the total number of multiple anode events) :

$$\begin{array}{l}\text{\% doubles kept} \\ \text{by anode} \\ \text{analysis}\end{array} = \frac{\text{\# (1,1) doubles}}{\text{\# multiple anode events}} \times 100 \quad .$$

Substituting for the # (1,1) doubles we get

$$(9) \quad \begin{array}{l}\text{\% doubles kept} \\ \text{by anode} \\ \text{analysis}\end{array} = \frac{\text{\# (1,1) events} > \text{large acp}}{\text{\# multiple anode events}} \times \frac{\text{\# (2,2) events total}}{\text{\# (2,2) events} > \text{large acp}} \times 100 \quad .$$

The ratios given in (8) and (9) are plotted in Figures 5 and 6 respectively for 28 MeV 0 Deg. data using various choices of the small and large a.c. pht. limits. Notice that the doubles kept ratio decreases sharply and then levels off as the large a.c. pht. limit is increased. The ratio falls because the number of singles above the limit falls sharply as we raise it, so the number

of events we call doubles (the # above the limit) is not as inflated by singles. The actual limit used to calculate the doubles kept ratio is 4000 in this case, where the ratio is about 6% (28 MeV 0 Deg.) . Similarly, the singles lost ratio falls as the limit is decreased. Again, this is because the number of doubles below the limit falls sharply as we lower the limit, so the number of events we call singles (the # below the limit) is not as inflated by doubles. The small a.c. pht. limit used to calculate the singles lost ratio is picked at 2500 (a conservative choice since it is not much below the singles/doubles cutoff, and is significantly above the single electron energy loss peak). The ratio at this limit is about 4% , i.e no more than ~4% of all the single electron events fire more than one anode wire.

We now need to calculate the singles lost and doubles kept ratio for the composite analysis :

$$\% \text{ doubles kept} = \begin{matrix} \% \text{ doubles kept} \\ \text{by anode} \\ \text{analysis} \end{matrix} \times \begin{matrix} \% \text{ doubles kept} \\ \text{by cathode} \\ \text{analysis} \end{matrix} \times \frac{1}{100}$$

$$100 - \% \text{ singles lost} = \left[100 - \begin{matrix} \% \text{ singles lost} \\ \text{due to anode} \\ \text{analysis} \end{matrix} \right] \times \left[100 - \begin{matrix} \% \text{ singles lost} \\ \text{due to cathode} \\ \text{analysis} \end{matrix} \right] \times \frac{1}{100}$$

These formulas hold since the anode and cathode analyses are independent. These six ratios, along with the total doubles contamination, are tabulated for various energies and angles in Table 2. The doubles contamination is defined as :

$$\begin{matrix} \% \text{ doubles} \\ \text{contamination} \end{matrix} = \begin{matrix} \% \text{ doubles} \\ \text{kept} \end{matrix} \times \frac{\text{total doubles}}{\text{total singles}}$$

$$\approx \quad \begin{array}{c} \% \text{ doubles} \\ \text{kept} \end{array} \quad \times \quad \frac{\# \text{ multiple anode events}}{\# \ (1,1) \text{ events}} \quad .$$

V. Nonuniform Beam Correction

In section II, we found that the angular response function could be written as (equation 3)

$$\tau_{1-N}(E_0, \vartheta_0) = \frac{A_{1-N}(E_0, \vartheta_0)}{A\Omega_{1-N} J_0} .$$

This equation was derived assuming a uniform beam. However, the accelerator beam is not uniform. Since the proportional counter in front of TET measures the x and y position of each incident electron, we have the information necessary to correct for the nonuniformity of the beam. The angular response function $\tau_{1-N}(E_0, \vartheta_0)$ for the case of a nonuniform beam is given by

$$(10) \qquad \tau_{1-N}(E_0, \vartheta_0) = \frac{1}{A\Omega_{1-N}} \int_{-\infty}^{\infty} \int_{-\infty}^{\infty} \frac{A_{1-N}(E_0, \vartheta_0, x, y)}{J_0(x, y)} dx dy .$$

where $J_0(x,y)dxdy$ is the number of electrons per second incident on the proportional counter at x,y within dxdy and $A_{1-N}(E_0, \vartheta_0, x, y)dxdy$ is the number of electrons per second in range N that had a proportional counter position x,y within dxdy . The ratio of $A_{1-N}dxdy$ and J_0dxdy gives the probability that an electron at x,y within dxdy will be a range N event. Thus the integral measures the "effective area" of range N for electrons of incident energy E_0 and incident angle ϑ_0 . We can approximate the integral by a sum:

$$\tau_{1-N}(E_0, \vartheta_0) \approx \frac{1}{A\Omega_{1-N}} \sum_{i,j} \frac{A_{1-N}(E_0, \vartheta_0, x_i, y_j)}{J_0(x_i, y_j)} \Delta x \Delta y$$

where the x_i's and the y_j's are uniformly spaced with spacings of Δx and Δy , respectively. Thus, we divide up the area of the proportional counter into boxes and count the total number of events in a time interval Δt in each box to find $J_0(x_i, y_j)\Delta x \Delta y \Delta t$. Similarly, by counting the number of range N events in each box during the same time interval we measure

$A_{1-N}(E_0, \vartheta_0, x_i, y_j) \Delta x \Delta y \Delta t$. The $\Delta x \Delta y \Delta t$'s cancel when we take the ratio, so we find

$$(11) \qquad \tau_{1-N}(E_0, \vartheta_0) \approx \frac{1}{A\Omega_{1-N}} \sum_{i,j} \frac{\text{\# range N events in box i,j}}{\text{total \# events in box i,j}} \times \text{area of the box} \quad .$$

There are two sources of position information from the proportional counter that could be used to separate events into boxes. They are:

1) The anode wires

2) The four cathode pulse heights

The eight anode wires in each direction are spaced exactly $\frac{1}{2}$ inch apart ; hence the anode wires subdivide the proportional counter into 64 $\frac{1}{4}$ inch^2 squares. An electron incident on a square will always fire the same x,y anode wires, and, since multiple anode events are rejected by the doubles check, there is never any ambiguity about which box the event falls into. The X1, X2, Y1, and Y2 cathode pulse heights give the electron x,y position to first order as

$$(12a) \qquad x = \frac{X2}{X1 + X2}$$

$$(12b) \qquad y = \frac{Y2}{Y1 + Y2} \quad .$$

The values of x and y range between 0 and 1 . Therefore, the cathode pulse heights could potentially be used to divide the proportional counter in a very fine grid. The problem with this method, however, is that the actual position is not exactly as given in equations 12. The relationship between the pulse heights and the position can, of course, be calibrated using the anode wires, but rather than do this, we decided to use the anode wires directly to divide the proportional counter. The anode boxes are a reasonable size (they are small enough so that it takes about 10 boxes to cover TET, but large enough so that there are typically 1000 events in each box), they require no calibration, and their area is precisely known. The final response

equation with this method is

$$(13) \qquad \tau_{1-N}(E_0, \vartheta_0) \;\approx\; \frac{1}{A\Omega_{1-N}} \times .25 \text{ in.}^2 \times \sum_{i,j} \frac{\text{\# range N events that fired anode wires i,j}}{\text{total \# events that fired anode wires i,j}} \qquad .$$

In the analysis programs, the normalizing factor $\frac{1}{A\Omega_{1-N}} \times .25$ in.^{2} is omitted (to be put in later).

VI. Guard RF Pickup Problem

A problem one has to deal with when working with a linear accelerator is RF pickup. Basically, the electromagnetic wave which accelerates the particles induces spurious noise in the measurement electronics. In the case of the TET calibration, the guards were particularly sensitive to RF pickup because of their large effective areas. This was aggravated by the fact that the guard thresholds are set very low (200 keV vs. 500 keV for D1-D7), just above the detector noise, and that each guard signal GA and GB is the sum of the signals from four guard rings. Figure 7a shows an oscilloscope pattern made by the RF noise on the Y2 proportional counter cathode postamp output. (Unfortunately, there are no pictures of the guard noise. However, a sketch in the run notebook (p. 54) indicates that the guard noise was fairly similar to the Y2 noise.) The top trace, triggering the oscilloscope, is the so-called "beam gate", a signal provided by the accelerator to inform the experimental electronics that electrons are on their way, and the bottom trace is the Y2 proportional counter output. The proportional counter was not biased, so that we only see the RF-induced signal. The key thing to notice is that the RF induces a definite nonrandom wave form, one that is the same for all beam dumps. The typical amplifier shaping time for an electron going through the proportional counter or a detector is about 2 μs, as shown in Figure 7b, which is narrow relative to the RF noise waveform. Therefore, the RF signal does not average out over the duration of the pulse, but instead generally adds to the pulse. Since the RF signal has a definite shape, the amount added does not vary significantly.

Figure 8a shows the GA pulse height distribution in the interval $0 \leq GA \leq 1000$ for electrons of energy 15 MeV and angle 20° relative to the telescope axis. Since the pulse height is a 13-bit number (i.e maximum value 8191), we are looking at the low pulse height portion of the distribution. What is observed is a large "detector noise" peak in channels 0-150. Most events fall into this peak. Since there are not very many other events, it is necessary to expand the vertical scale to see them. Furthermore, to see large pulse height events it is

necessary to look at a larger interval of pulse heights. Figure 8b shows a GA 15 MeV 20°
distribution in the interval $0 \leq GA \leq 8000$. Besides the low channel peak, we see a peak
centered at about channel 910, corresponding to an energy loss of about 1.1 MeV. This is the
energy loss one expects for a relativistic electron traveling through a guard (.325 cm silicon).
Figure 9 shows a plot of GB in the interval $0 \leq GB \leq 8000$ for 28 MeV 0°. Four equally spaced
peaks are visible, corresponding to an electron penetrating one, two, three, or all four guards.
The higher peaks are not visible in Figure 8b since the beam was incident at an angle of 20° ,
making multi-guard events unlikely .

Now, for comparison, the low channel GA pulse height distribution for 72 MeV 20°
electrons is shown in Figure 10a. The low energy noise peak is shifted upwards compared to
Figure 8a. Figure 10b shows the overall GA pulse height distribution ($0 \leq GA \leq 8000$). The peak
corresponding to an electron penetrating a single guard detector is also shifted upwards,
compared to Figure 8b, to approximately channel 980. At first, one might think that the shift
in the penetrating peak is due to an actual increase in the energy loss in a guard. However,
detailed studies show that the energy loss in D1 does not vary appreciably over the 6-72 MeV
energy range, in contrast to the Landau energy loss predictions. (See N.G.'s Voyager notebook
2/18/79 - 4/2/80 ; a possible explanation is that knock-on electrons escaping out the back of
the detector carry away enough energy to cancel the relativistic rise in the energy loss.)
There has to be another explanation for the shift. We can calculate how much the peak has
shifted by subtracting the mean of the energy loss peak at 15 MeV from the mean of the
energy loss peak at 72 MeV. We find that this shift (70 channels) is nearly the same as the shift
in the low channel "detector noise" peak (65 channels). Moreover, the energy loss peak is not
appreciably wider at 72 MeV than at 15 MeV. The detector noise and energy loss shifts were
calculated at several energies for both GA and GB ; in each case the shifts were approximately
equal. This suggests that the whole pulse height distribution has been shifted a constant
amount by the RF signal. This is the the same conclusion that was arrived at earlier by looking
at the RF signal itself. The reason a shift is apparent at the higher energies and not lower

energies is that a larger RF power is required to accelerate the higher energy electrons, so the amplitude of the RF pickup signal is correspondingly higher.

This pulse height shift causes a problem because the guard threshold did not shift correspondingly. Hence, more events triggered the guard threshold than normally would have without the RF noise. It was therefore necessary to ignore the guard tag when processing the data, and use the actual pulse heights instead. For each energy, a corrected guard threshold was calculated by measuring the shift of the detector noise peak relative to the location of the peak at some noise-free energy, and then adding this shift to the original threshold (200 keV) . Table 3 lists the calculated thresholds for all energies. The GB thresholds for 6-11 MeV are very low because the amplifier gain was turned down by a factor of 2 at these energies. Thus the threshold for GB at 11 MeV is actually $2 \times 87 = 174$. The table shows that RF pickup was a problem only for electron energies of 39, 53, and 72 MeV. The "noise-free" energies were chosen to be 28 MeV for GA and 21 MeV for GB because the detector noise peaks had the smallest means at these energies. When analyzing the data, the guard pulse heights were compared to the corrected threshold. If either GA or GB exceeded its respective threshhold, the event was counted as a real guard event and therefore thrown out.

VII. Angular Integration of the Response

In section III, we found that the telescope's response to an isotropic flux could be written (equation 5, p. 8)

$$R_{1-N}(E) \; = \; 2\pi \int\limits_0^\pi \tau_{1-N}(E,\vartheta)\sin(\vartheta)d\vartheta \quad .$$

Since $\tau_{1-N}(E,\vartheta)$ is measured , the objective is to perform the integral. However, $\tau_{1-N}(E,\vartheta)$ is measured only for certain values of E (6, 8, 11, 15, 21, 28, 39, 53 and 72 MeV). Furthermore, for each energy E, $\tau_{1-N}(E,\vartheta)$ is known only for a few values of ϑ. The specific values vary, but a typical set is $\vartheta=$ 0, 10, 20, 30, 40, 50, 60, and 90 degrees. (The response was assumed to be zero between 90 and 180 degrees.) Hence the integration cannot be performed exactly, but must be approximated numerically. The rest of this section describes how this was done.

A general way to perform the integration is to fit a function $f(\vartheta)$ to the experimental values of $\tau_{1-N}(E,\vartheta)$. Since $f(\vartheta)$ is then known for all values of ϑ, the integration (where $\tau_{1-N}(E,\vartheta)$ is replaced by $f(\vartheta)$) can be performed exactly. The fitting function in our case was chosen to be linear; that is

$$f_r(\vartheta) \; = \; a\vartheta + b \; , \quad \vartheta_r < \vartheta < \vartheta_{r+1}$$

where a and b are determined by $\tau_{1-N}(E,\vartheta_r)$ and $\tau_{1-N}(E,\vartheta_{r+1})$. Higher order polynomials were also tried, but were found to give non-physical peaks and valleys in some cases. A check was made to see what effect the order of the interpolating polynomial has on the value of the integral for the cases where good higher order polynomial fits were obtained. Table 4 shows that the variation is quite small, and therefore that a linear fit is adequate.

Even with the linear fit, a problem arose in the large angle region. The angular response typically has a steep downward slope in the intermediate region ($40°\leq\vartheta\leq60°$), but at the last

point before 90° (usually 50° or 60°) the response is still fairly sizeable (see Figure 11a). Since a linear fit was done between 60° and 90° (no intermediate points were measured), the fitted response would be higher in this region than we felt it should be. The real response probably continues falling steeply past 60°, approaching some small value between 65° and 75°. The problem was compounded by the fact that the $\sin(\vartheta)$ factor weights the large angle region more than the small angle region. For these reasons it was decided to "add" a data point in the large angle region. This point is placed at the intersection of the line formed by the two points prior to the 90° point and a horizontal line having a distance from the ϑ - axis equal to the value of the 90° response (see Figure 11b). The added point thus continues the downward trend in the response until it reaches a reasonably low level. The point is added only if the intersection is between the last two points (i.e. between 50° or 60° and 90°). Plots of the resulting response functions (along with the original data points) were made for each energy and range, and can be found in the Angular Response Plots notebook in Room 207 (or see A. Cummings).

VIII. Results and Conclusions

The TET isotropic response functions, $R_{1-N}(E)$, for ranges three through seven as determined by the above analysis are shown in Figure 12. The values of the points and errors shown in the figure are listed in Table 5. Given these response functions and an electron spectrum, $\frac{dJ}{dE}(E)$, the counting rate in each TET range can be determined using equation 1,

$$(1) \qquad D_{1-N} \;=\; A\Omega_{1-N} \int_0^{\infty} \frac{dJ}{dE}(E)\; R_{1-N}(E)\; dE \;.$$

Reversing the problem, given the counting rate and the response functions, the value of the spectrum at five energies (the five D_{1-N} represent five degrees of freedom) can be calulated using a technique such as that described by Whitcomb [1973]. Equation 1 shows that $R_{1-N}(E)$ is the effective geometry factor as a function of energy of range 1-N divided by the physical geometry factor of that range, $A\Omega_{1-N}$ (Table 1), for normalization. Note that the only discriminator threshold requirement specified in the data analysis to produce these curves was that the event trigger the detector lower threshold (200 keV for GA, GB, and D8, and 500 keV for D1-D7). Response curves were also calculated using the 2.5 MeV upper limit imposed by the flight electronics on D1 and D2 pulse heights. These response curves are listed in Table 6. If upper thresholds for D3-D7 and more restricted D1 and D2 pulse height windows are desired, new response curves must be generated. Generating new curves is not difficult, however, since the programs are modularized and well documented. The program tapes, listings, and documentation notebooks are in Room 207 (or see A. Cummings).

Appendix A: The Proportional Counter

For the TET electron calibration, a multiwire proportional counter was used to determine the positions of the electrons and to separate double electron events from single electron events. The proportional counter (PC) consists of two pairs of anode and cathode planes. The anode planes have 24 equally spaced thin (20 μm diameter) wires which are biased at positive high voltage. The wire spacing is exactly 1/6" . Adjacent wires are tied together in groups of three to form eight outputs. Instead of wires, the cathode planes have 48 aluminized strips (which are perpendicular to the corresponding anode wires) on a 1/2 mil mylar sheet. These strips are resistively coupled to ground, and each strip is connected to the two neighboring strips with 4700 pF capacitors. Extra capacitors connected to each of the two end strips form the outputs of the cathode plane.

The two pairs of anode/cathode planes are separated by a ground plane made of a 1/4 mil aluminized mylar sheet. 1/4 mil aluminized mylar ground planes also separate the anode planes from the gas windows, which are also 1/4 mil aluminized mylar. (i.e., the arrangement from front to back is gas window, ground plane, anode plane, cathode plane, ground plane, cathode plane, anode plane, ground plane, and gas window.) The two halves of the chamber are oriented perpendicularly to one another, so that the two anode planes and the two cathode planes can be used independently to obtain x-y position information.

An electron traveling through the PC ionizes gas atoms along its trajectory. The ionized electrons and the secondary electrons that they create then drift toward the nearest anode wire, and the standard proportional counter multiplication takes place, leaving behind positive ions around the wire. Since these ions are heavy, their drift velocities are much slower than the electron drift velocities, and they thus remain close to the wire for some time after all of the electrons have been collected. This net positive charge along the wire induces a negative image charge on the cathode strips. The way that the outputs of the cathode plane are related to this image charge and the way that the outputs can be used to get position

information will be described later.

Since adjacent anode wires are tied together in groups of three, the spatial resolution of the anode planes is no better than the wire group spacing, which is 1/2" . However, since the drift paths of the secondary electrons are perpendicular to the anode wire, the location of the positive ions parallel to the wire is the same as the parallel location of the incident particle. The cathode plane measures this parallel position with a resolution of approximately 1 mm. For example, if the anode wires run parallel to an "x" axis, and the cathode strips run parallel to a "y" axis, then the anode wires give crude position information in the y direction, and the cathode strips give precise position information in the x direction.

The outputs of the cathode planes are successively amplified by TC 164 charge sensitive preamps followed by TC 213 postamps. The TC 213 postamp outputs are then pulse height analyzed by PACE (1st 4 PACE channels). The anode signals are not pulse height analyzed, but are compared to a threshold in a discriminator circuit. The threshold was set low enough that minimum-ionizing electrons could fire the discriminator, but high enough that the region between wires where both wires are fired was minimized. The discriminator outputs (16 in all; 8 for each anode plane) form the external word input to PACE.

We will now derive the relation between the induced image charge on the cathode and the cathode outputs, and determine the equation that relates the cathode outputs to a position measurement.
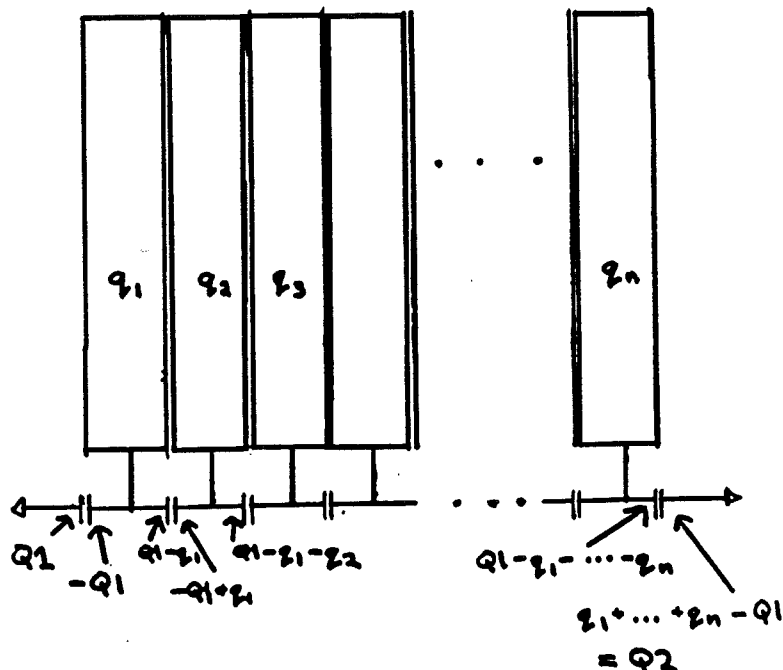
Suppose that the positive ions left behind by the multiplication process induce image charges $q_1, q_2, \cdots, q_n$ on the cathode strips. We would like to find Q1 and Q2, the charges on the preamp sides of the two end capacitors. To do this, we find the charges on all the capacitors, and then use the condition that the preamp inputs are at ground potential. First of all, we look at the first strip. The preamp side of the output capacitor has a charge defined as Q1. Therefore, the "strip" side of this capacitor has charge -Q1. Now we look at the capacitor joining strips 1 and 2, which we shall call C12. By conservation of charge (assuming that the resistor to ground has not allowed an appreciable current to flow), the charge on the "1" side of C12 is $Q1 - q_1$, since the capacitors were uncharged before the image charges were induced (the resistors would have bled any charge off the capacitors). Now, the "2" side of C12 is charged with $-Q1 + q_1$, so the "2" side of C23 is charged with $Q1 - q_1 - q_2$. By repeating this argument, we find that the "strip" side of the output capacitor attached to the last strip has a charge of $Q1 - q_1 - q_2 - \cdots - q_n$, and thus $Q2 = q_1 + \cdots + q_n - Q1$. Using the condition that the preamp inputs are at ground, we get

$$0 = \frac{Q1}{C} + \frac{Q1-q_1}{C} + \cdots + \frac{Q1-q_1-\cdots-q_n}{C}$$

so

$$(n+1)Q1 = \sum_{k=1}^{n} (n+1-k)q_k$$

$$Q1 = \sum_{k=1}^{n} \frac{n+1-k}{n+1} q_k \quad .$$

Similarly,

$$Q2 = \sum_{k=1}^{n} \frac{k}{n+1} q_k.$$

so

$$Q1+Q2 = \sum_{k=1}^{n} \left[\frac{n+1-k}{n+1} q_k + \frac{k}{n+1} q_k \right]$$

$$= \sum_{k=1}^{n} q_k \quad .$$

Now we form the quantity

$$\frac{Q2}{Q1+Q2} = \frac{\sum_{k=1}^{n} \frac{k}{n+1} q_k}{\sum_{k=1}^{n} q_k} \quad .$$

$\frac{k}{n+1}$ is roughly the position of the k'th strip on a scale from 0 to 1. (The actual position of the

center of the strip is $\frac{k-\frac{1}{2}}{n}$ on a scale of 0 to 1.) Thus $\frac{Q2}{Q1+Q2}$ is the image-charge-weighted

average of the strip positions, and therefore gives the position of the incident electron (on a

scale of 0 to 1).

As an example of how one could actually calculate the image charge induced on the

cathode, we solve the following simplified electrostatic problem: consider the positive ion

cluster to be a point charge q at a distance d above the cathode plane; consider the cathode

plane to be an infinite, perfectly conducting sheet, and neglect the presence of other

conductors, such as the anode wires and the ground planes. Suppose the strips run in the y-

direction. We take an x-y coordinate system with the origin directly below the point q. Using

the method of images, we find the induced surface charge density to be

$$\sigma(x,y) = \frac{qd}{2\pi(d^2 + x^2 + y^2)^{3/2}} \quad .$$

If the k'th strip has boundaries at the x-coordinates x_k and $x_{k+1} = x_k+\Delta x$, we find

$$q_k = \int_{x_k}^{x_{k+1}} dx \int_{-\infty}^{\infty} dy \, \sigma(x,y)$$

$$= \frac{q}{\pi} \left[\tan^{-1}\left[\frac{x_{k+1}}{d}\right] - \tan^{-1}\left[\frac{x_k}{d}\right] \right] \quad .$$

The q_k's are found to be small except when x_k is close to 0, which is the x-coordinate of the point charge q.

Appendix B

For reference purposes, this appendix lists the PACE event format and a tape log.

Word

0	P.C. X1
1	P.C. X2
2	P.C. Y1
3	P.C. Y2
4	D1
5	D2
6	D3
7	D4
8	D5
9	D6
10	D7
11	D8
12	GA
13	GB
14	Internal Tag
15	External Tag
16	External Word

\# bytes per event = 34
\# events per record = 100

Pulse Heights:

Bits 0-13 - 13 bit pulse height (0 - 8191)
Bit   14 - overflow bit. Valid only if bit 16 is set.
Bit   15 - calibrate bit (not used in this calibration)
Bit   16 - LLD bit. Set only if Lower Level Discriminator for this
            channel fired. Also stored in Internal Tag (see below).

Internal Tag:

__ __ GB GA D8 D7 D6 D5 D4 D3 D2 D1 Y2 Y1 X2 X1

most significant   least significant

Each bit is 1 or 0 according to whether the corresponding PACE channel LLD fired or not.

External Tag:

    Bit 0 - beam gate
    Bit 1 - set if any anode wire fired

External word:

    $\underline{Y8}$ $\underline{Y7}$ $\underline{Y6}$ $\underline{Y5}$ $\underline{Y4}$ $\underline{Y3}$ $\underline{Y2}$ $\underline{Y1}$ $\underline{X8}$ $\underline{X7}$ $\underline{X6}$ $\underline{X5}$ $\underline{X4}$ $\underline{X3}$ $\underline{X2}$ $\underline{X1}$

Each bit is 1 or 0 according to whether the corresponding proportional
counter anode discriminator fired or not.

File format: EOF
                    header record
                    event record

                    . . .

                    event record
                    trailer record
                      EOF

There are approximately 100 event records per file.

Tape Log

et305

Energy	GA thresh	GB thresh	Angle	Start File	No. Files	S/D Cutoff
28	172	192				
			0	1	6	3000
			5	7	6	3000
			10	13	6	2900
			15	19	6	2800
			20	25	6	2800
			25	31	6	2600
			30	37	6	2600
			35	45	6	2700
			40	51	6	2700
			45	57	6	2700
			50	63	6	2700

tet306

Energy	GA thresh	GB thresh	Angle	Start File	No. Files	S/D Cutoff
28	172	192				
			90	3	20	2800
39	186	226				
			0	44	6	3000
			5	50	6	3100

tet307

Energy	GA thresh	GB thresh	Angle	Start File	No. Files	S/D Cutoff
39	186	226				
			10	1	6	3200
			15	7	6	3200
			20	13	6	3200
			25	19	6	3200
			30	25	6	3200
			35	31	6	3200
			40	37	6	3200
			45	43	6	3200
			50	49	6	3200

tet308

Energy	GA thresh	GB thresh	Angle	Start File	No. Files	S/D Cutoff
39	186	226				
			90	1	19	3200

tet312

Energy	GA thresh	GB thresh	Angle	Start File	No. Files	S/D Cutoff
53	190	218				
			0	20	6	3100
			5	26	6	3100
			10	32	11	3100
			15	43	11	3100

Tape Log

tet313

Energy	GA thresh	GB thresh	Angle	Start File	No. Files	S/D Cutoff
53	190	218				
			20	1	11	3100
			25	12	11	3100
			30	23	11	3100
			40	34	6	3100
			90	40	18	3100

tet314

Energy	GA thresh	GB thresh	Angle	Start File	No. Files	S/D Cutoff
72	239	328				
			0	29	14	3000
			5	43	9	3000

tet315

Energy	GA thresh	GB thresh	Angle	Start File	No. Files	S/D Cutoff
72	239	328				
			10	1	17	3000
			15	18	17	3000
			20	35	17	3000

tet316

Energy	GA thresh	GB thresh	Angle	Start File	No. Files	S/D Cutoff
72	239	328				
			25	1	17	3000
			30	18	17	3000
			40	35	9	3000
			90	44	5	2600

tet317

Energy	GA thresh	GB thresh	Angle	Start File	No. Files	S/D Cutoff
72	239	328				
			90	1	27	3000

Tape Log

tet420

Energy	GA thresh	GB thresh	Angle	Start File	No. Files	S/D Cutoff
6	175	89				
			0	1	11	3100
			10	12	14	3100
			20	26	14	3100
			30	40	14	3100

tet321

Energy	GA thresh	GB thresh	Angle	Start File	No. Files	S/D Cutoff
6	175	89				
			40	1	8	3100
			50	9	8	3100
			60	17	8	3100
			90	25	9	3100

tet322

Energy	GA thresh	GB thresh	Angle	Start File	No. Files	S/D Cutoff
8	175	88				
			0	1	8	3200
			10	9	14	3200
			20	23	12	3200
			30	35	14	3200
			40	49	8	3100

tet323

Energy	GA thresh	GB thresh	Angle	Start File	No. Files	S/D Cutoff
8	175	88				
			50	1	8	3100
			60	9	8	3200
			90	17	12	3200

tet424

Energy	GA thresh	GB thresh	Angle	Start File	No. Files	S/D Cutoff
11	176	87				
			0	11	8	3200
			10	19	14	3200
			20	33	14	3200
			30	47	11	3200

Tape Log

tet325

Energy	GA thresh	GB thresh	Angle	Start File	No. Files	S/D Cutoff
11	176	87				
			40	1	8	3200
			50	9	8	3200
			60	17	8	3200
			90	25	11	3200

tet426

Energy	GA thresh	GB thresh	Angle	Start File	No. Files	S/D Cutoff
15	174	172				
			0	7	9	3200
			10	16	14	3200
			20	30	14	3200
			30	44	14	3200
			40	58	3	3200

tet427

Energy	GA thresh	GB thresh	Angle	Start File	No. Files	S/D Cutoff
15	174	172				
			40	1	8	3200
			50	9	8	3200
			60	17	8	3100
			90	25	12	3200

tet428

Energy	GA thresh	GB thresh	Angle	Start File	No. Files	S/D Cutoff
21	175	172				
			0	12	12	3400
			10	24	20	3400
			20	44	15	3400

tet429

Energy	GA thresh	GB thresh	Angle	Start File	No. Files	S/D Cutoff
21	175	172				
			20	1	11	3400
			30	12	14	3400
			40	26	11	3400
			50	37	11	3400
			90	48	13	3400

References

Rossi, B., *High-Energy Particles*, Prentice-Hall, New Jersey, 1952.

Stone, E.C., R.E. Vogt, F.B. McDonald, B.J. Teegarden, J.H. Trainor,
J.R. Jokipii and W.R. Webber, Cosmic Ray Investigation for the
Voyager Missions: Energetic Particle Studies in the Outer Heliosphere -
and Beyond, Sp. Sci. Rev, *21*, 355, 1977.

Whitcomb, S., Design of a Cosmic Ray Electron Energy Spectrometer for
use in Deep Space, SRL internal report #8, 1973.

Figure Captions

Figure 1   Schematic diagram of TET.

Figure 2   Diagram of equipment setup at La Jolla accelerator
            calibration. Not to scale.

Figure 3   Average proportional counter cathode pulse height
            ((X1+X2+Y1+Y2)/4) distributions for a) (2,2) anode requirement
            (mostly double electron events), b) (1,1) anode requirement
            (mostly single electron events), and c) no anode requirement.

Figure 4   Percent singles lost and percent doubles kept by the
            cathode analysis vs. s/d cutoff. The dashed lines indicate
            the % singles lost (4.3%) and the percent doubles kept (12%)
            at the chosen s/d cutoff (3000).

Figure 5   Percent doubles kept by the anode analysis vs. large
            average cathode pulse height limit (see section IV).
            Notice that the % doubles kept levels off at about 6% .

Figure 6   Percent singles lost by the anode analysis vs. small
            average cathode pulse height limit (see section IV).

Figure 7   Oscilloscope pictures of the beam gate and Y2 postamp
            signals. In a), the proportional counter is not biased, so we
            see the RF noise induced in Y2. In b), the PC is biased, so
            we see the signal from electrons going through the PC.

Figure 8   GA pulse height distributions for 15 MeV 20 degrees.
            The entire distribution is shown in b), while a) shows only
            the low pulse height portion.

Figure 9   GB pulse height distribution for 28 MeV 0 degrees.
            The peaks corresponding to an electron penetrating one,
            two, three, or all four of the guard detectors in GB are
            shown.

Figure 10   Same as Figure 8, except the electron energy is 72 MeV.

Figure 11   Angular response of D1-2 at 6 MeV. Figure 11b) shows
            the extra point determined by the program to give a more
            physical fitting function.

Figure 12   The TET isotropic response curves for ranges three
            through seven (no D1 or D2 upper limits). The exact values and
            errors of the points shown are listed in Table 5. Curves are
            drawn through the points to guide the eye. The errors represent
            the statistical counting uncertainties of the measurement
            at each energy and range propagated numerically through the
            angular integration.

Table 1

Geometry Factors

Range	Geometry Factor* (cm**2-sr)
D1	14.21
D1-2	3.12
D1-3	2.14
D1-4	1.53
D1-5	1.14
D1-6	0.86
D1-7	0.66
D1-8	0.50

* geometry factor of two separated disks

Table 2

Doubles Kept / Singles Lost

Energy	anode analysis		cathode analysis		combined		
	doubles kept	singles lost	doubles kept	singles lost	doubles kept	singles lost	doubles contamination
6 MeV	8.53 %	4.23 %	10.7 %	6.81 %	0.91 %	10.75%	0.25 %
15 MeV	7.28 %	3.43 %	10.8 %	4.70 %	0.79 %	7.97 %	0.17 %
28 MeV	6.00 %	3.78 %	12.0 %	4.25 %	0.72 %	7.87 %	0.22 %
72 MeV	4.47 %	3.78 %	11.0 %	4.27 %	0.49 %	7.89 %	0.23 %

Table 3

Guard Thresholds

Energy	GA	GB
6	175	89
8	175	88
11	176	87
15	174	172
21	175	172
28	172	192
39	186	226
53	190	218
72	239	328

Note: The GB gain was decreased by a factor
of 2 for the 6, 8, and 11 MeV runs.

Table 4

Integral of Angular Response For
Several Interpolating Polynomials

degree of polynomial,	Integral (not normalized)				
	D1-2	D1-3	D1-4	D1-5	D1-6
1 (linear)	0.1429	0.08596	0.06230	0.04462	0.00966
3 (cubic)	0.1432	0.08576	0.06217	0.04428	0.00957
5	0.1436	0.08574	0.06254	0.04434	0.00958
maximum difference	0.49 %	0.26 %	0.60 %	0.77 %	0.91 %

Table 5

TET Response Curves
No D1, D2 Requirement

				Electron Energy (MeV)					
	6	8	11	15	21	28	39	53	72
R1-2	0.5220	0.3742	0.1595	0.0832	0.0455	0.0409	0.0273	0.0225	0.0220
Error	0.0078	0.0060	0.0053	0.0029	0.0029	0.0040	0.0021	0.0033	0.0035
R1-3	0.1308	0.3553	0.3532	0.2224	0.0936	0.0682	0.0407	0.0275	0.0219
Error	0.0038	0.0054	0.0072	0.0064	0.0035	0.0046	0.0032	0.0030	0.0031
R1-4	0.0	0.0027	0.1046	0.2757	0.2117	0.1359	0.0839	0.0497	0.0301
Error	0.0	0.0004	0.0041	0.0050	0.0048	0.0049	0.0046	0.0030	0.0023
R1-5	0.0	0.0	0.0008	0.0204	0.1174	0.2093	0.1654	0.1021	0.0594
Error	0.0	0.0	0.0003	0.0014	0.0033	0.0059	0.0053	0.0032	0.0022
R1-6	0.0	0.0	0.0	0.0	0.0048	0.0769	0.1473	0.1392	0.1017
Error	0.0	0.0	0.0	0.0	0.0007	0.0040	0.0049	0.0038	0.0030
R1-7	0.0	0.0	0.0	0.0	0.0	0.0041	0.0457	0.0859	0.1122
Error	0.0	0.0	0.0	0.0	0.0	0.0010	0.0029	0.0032	0.0035
R1-8	0.0	0.0	0.0	0.0	0.0	0.0004	0.0047	0.0206	0.0731
Error	0.0	0.0	0.0	0.0	0.0	0.0003	0.0011	0.0016	0.0031

Table 6

TET Response Curves
D1, D2 < 2.5 MeV

	Electron Energy (MeV)								
	6	8	11	15	21	28	39	53	72
R1-2	0.3094	0.1805	0.0782	0.0445	0.0305	0.0282	0.0179	0.0147	0.0148
Error	0.0058	0.0039	0.0034	0.0019	0.0024	0.0031	0.0018	0.0026	0.0030
R1-3	0.1308	0.3483	0.3305	0.1998	0.0834	0.0587	0.0376	0.0235	0.0189
Error	0.0038	0.0053	0.0069	0.0062	0.0034	0.0041	0.0031	0.0024	0.0029
R1-4	0.0	0.0027	0.1040	0.2677	0.2024	0.1281	0.0769	0.0460	0.0272
Error	0.0	0.0004	0.0040	0.0049	0.0047	0.0048	0.0034	0.0029	0.0020
R1-5	0.0	0.0	0.0008	0.0202	0.1131	0.1993	0.1548	0.0985	0.0557
Error	0.0	0.0	0.0003	0.0014	0.0032	0.0057	0.0045	0.0032	0.0021
R1-6	0.0	0.0	0.0	0.0	0.0048	0.0746	0.1415	0.1339	0.0985
Error	0.0	0.0	0.0	0.0	0.0007	0.0040	0.0047	0.0037	0.0029
R1-7	0.0	0.0	0.0	0.0	0.0	0.0041	0.0447	0.0826	0.1077
Error	0.0	0.0	0.0	0.0	0.0	0.0010	0.0029	0.0031	0.0034
R1-8	0.0	0.0	0.0	0.0	0.0	0.0004	0.0047	0.0204	0.0722
Error	0.0	0.0	0.0	0.0	0.0	0.0003	0.0011	0.0016	0.0030
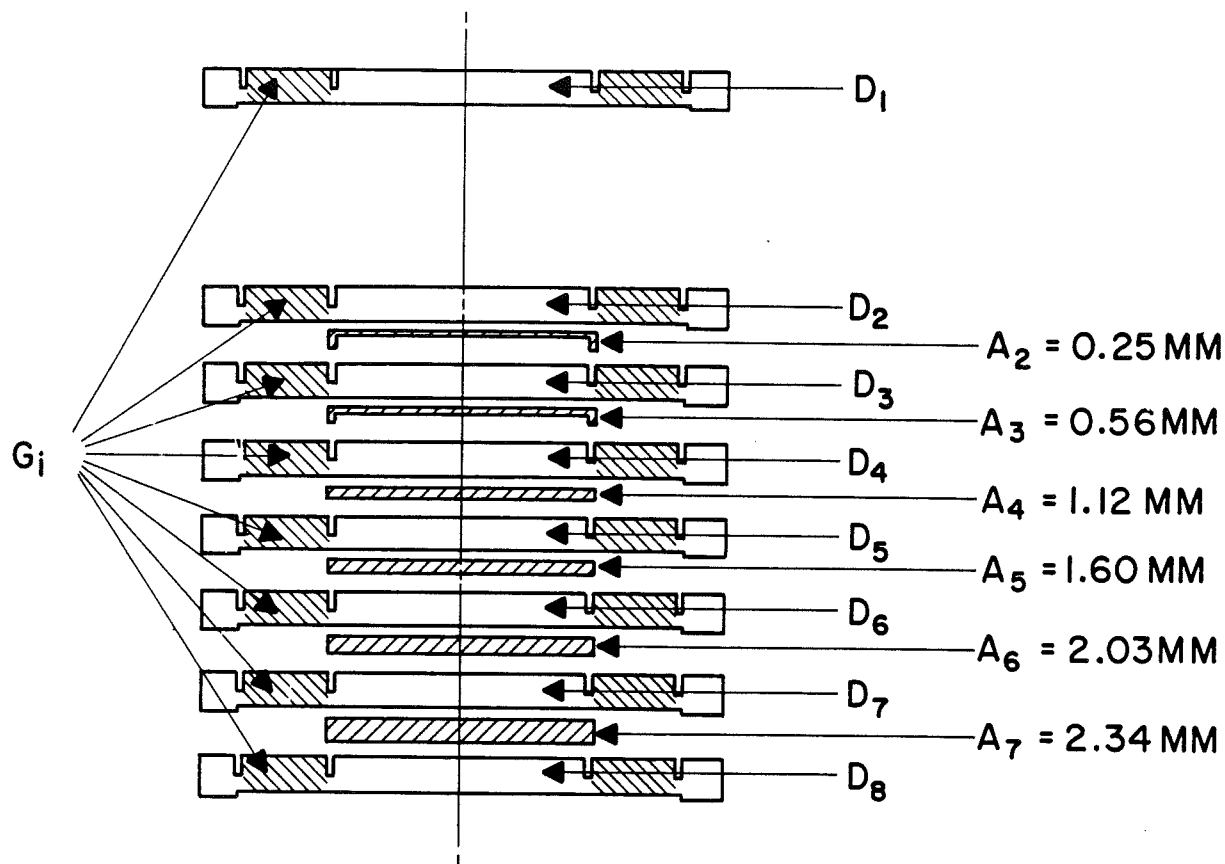
D_i = DETECTORS , 4.5 CM^2 x 3.0 MM , LiD

A_i = TUNGSTEN ABSORBER (ρ = 18.0 g / CM^3)

G_i = GUARD DETECTORS , 3.0 MM , LiD

THE ELECTRON TELESCOPE (TET)

GA = G1 + G3 + G5 + G7

GB = G2 + G4 + G6 + G8

Figure 1

Figure 2

COUNTS

Average Cathode Pulse Height (ch. #)

Figures 3a, 3b, 3c
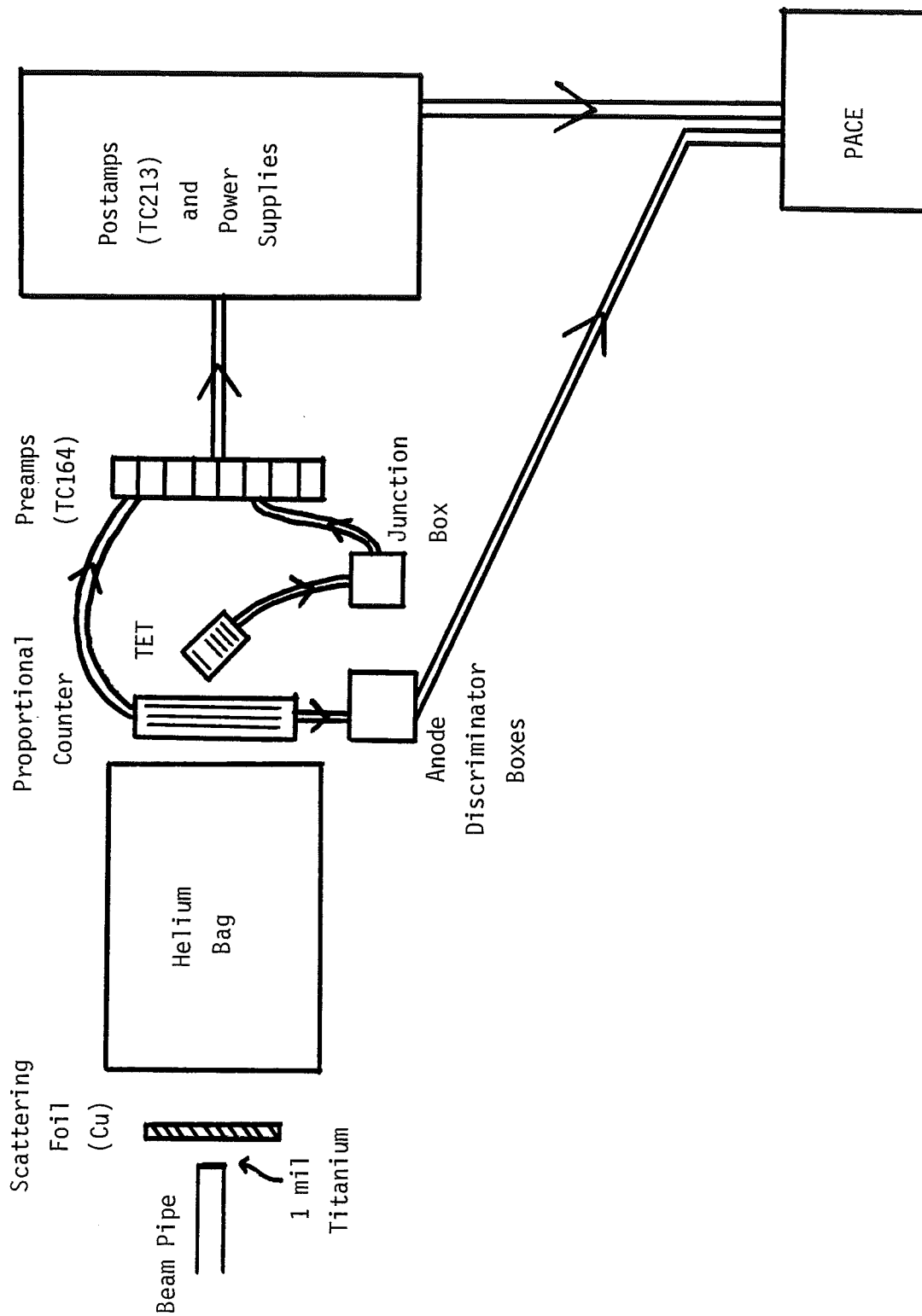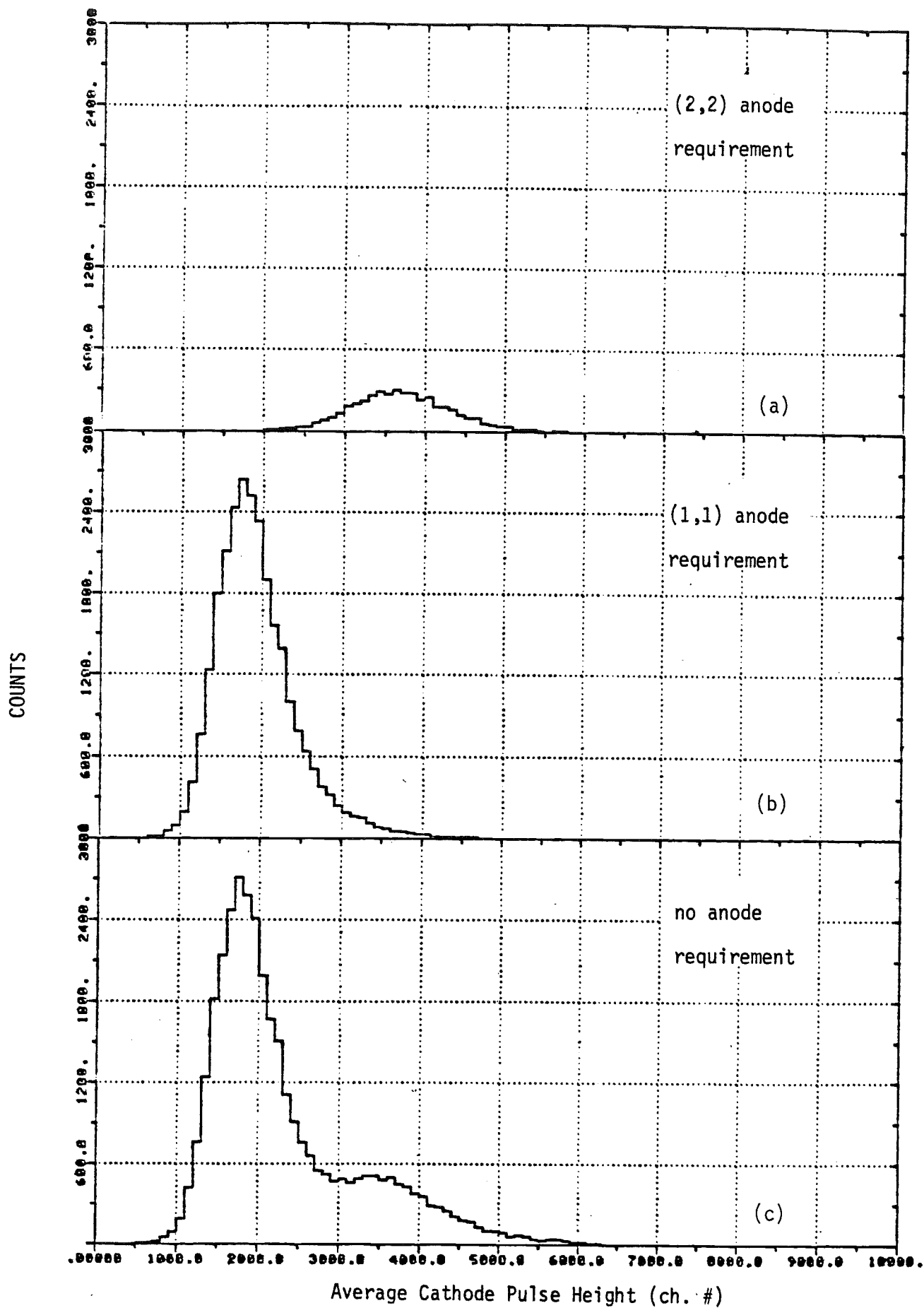
Average Cathode Pulse Height
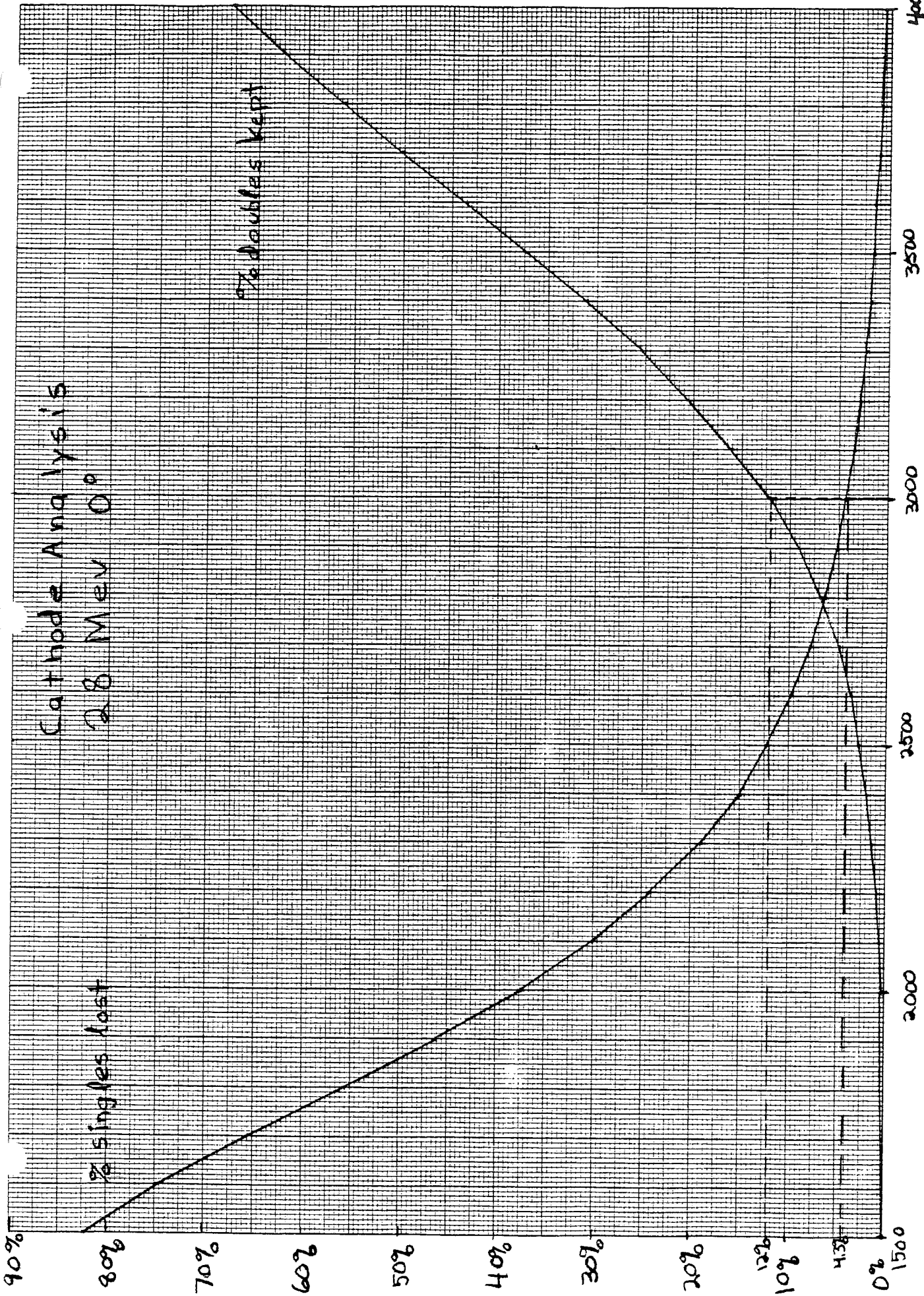
K+E   10 X 10 TO THE CENTIMETER   18 X 25 CM.
      KEUFFEL & ESSER CO. MADE IN U.S.A.

Figure 4   46 1510

Cathode Analysis
2.8 Mev 0°

% doubles kept

% singles lost

Figure 5

large average cathode pulse height limit
(large acp)

Anode Analysis
0.8 Mev 0°

% doubles kept
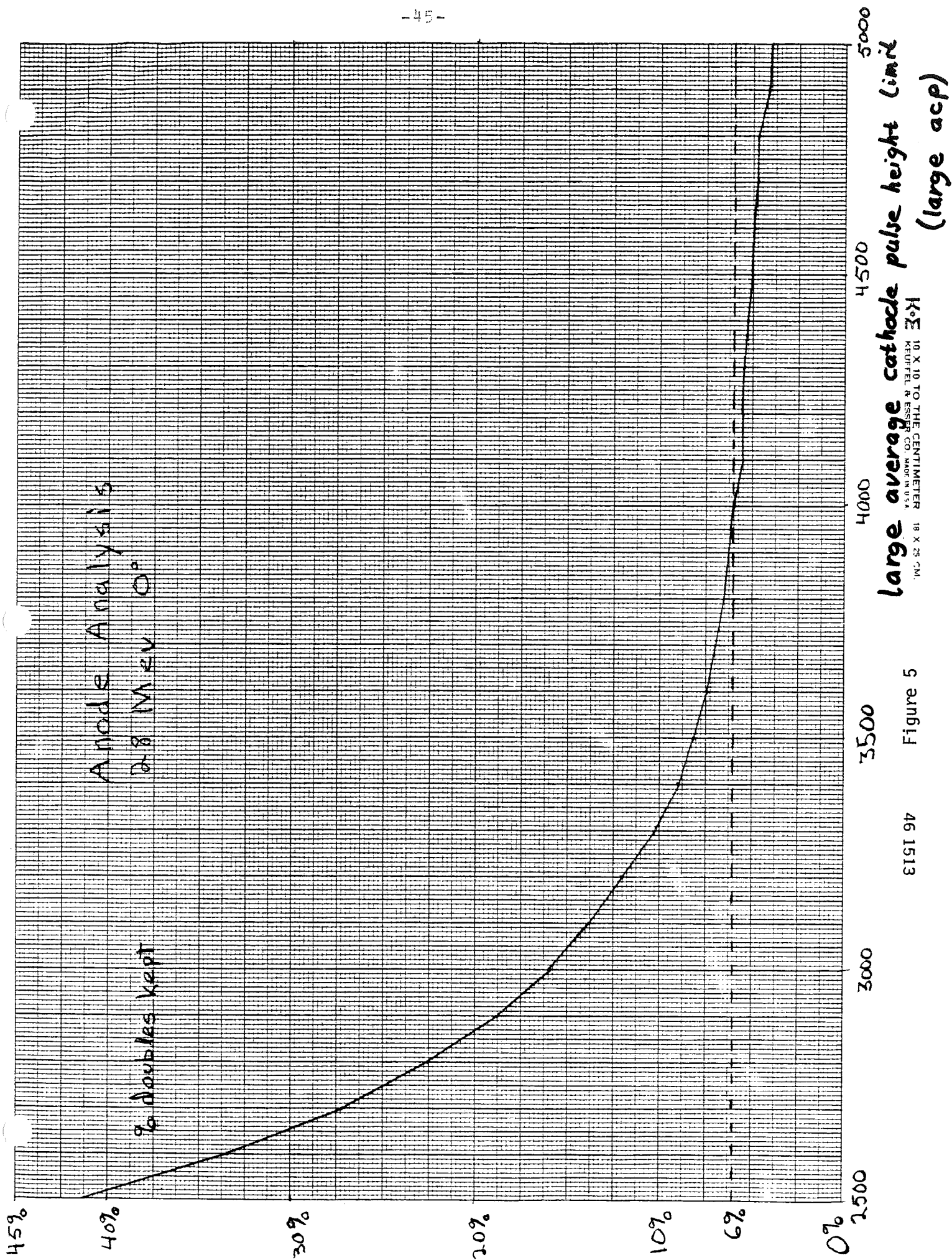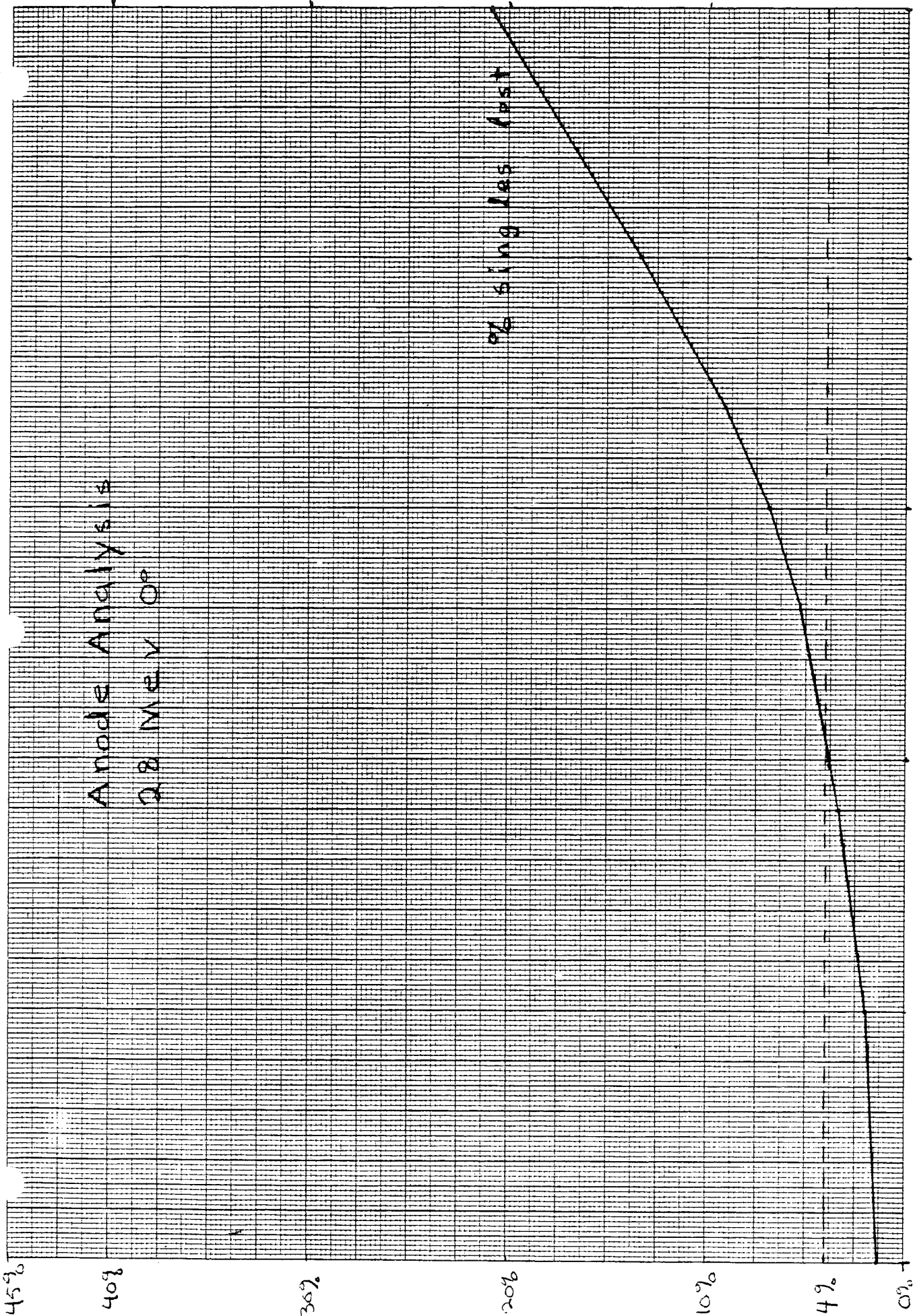
46 1513

Small average cathode pulse height (Small acp)

Anode Analysis
28 MeV 0°

Figure 9   46 1513

5 volts/division
Beam Gate

20 millivolts/division
Y2 (without bias)
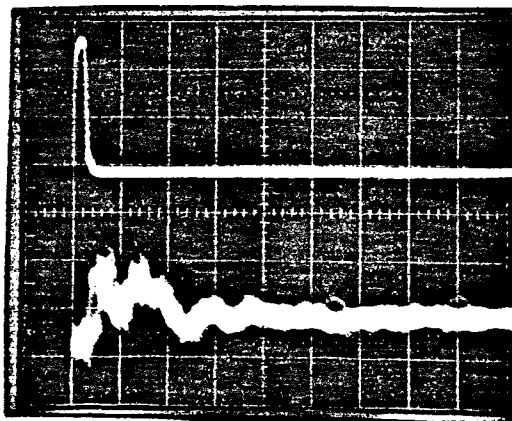
(RF noise)

5 microseconds/division

Figure 7a

5 volts/division
Beam Gate

1 volt/division
Y2 (with bias)
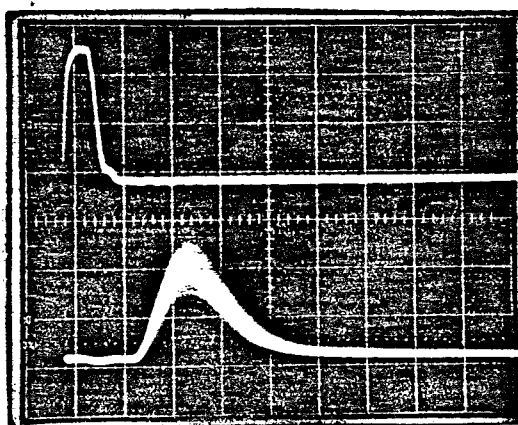
(electrons)

2 microseconds/division

Figure 7b

Channel Number

Figure 8a

mean = ch. 910   Channel Number
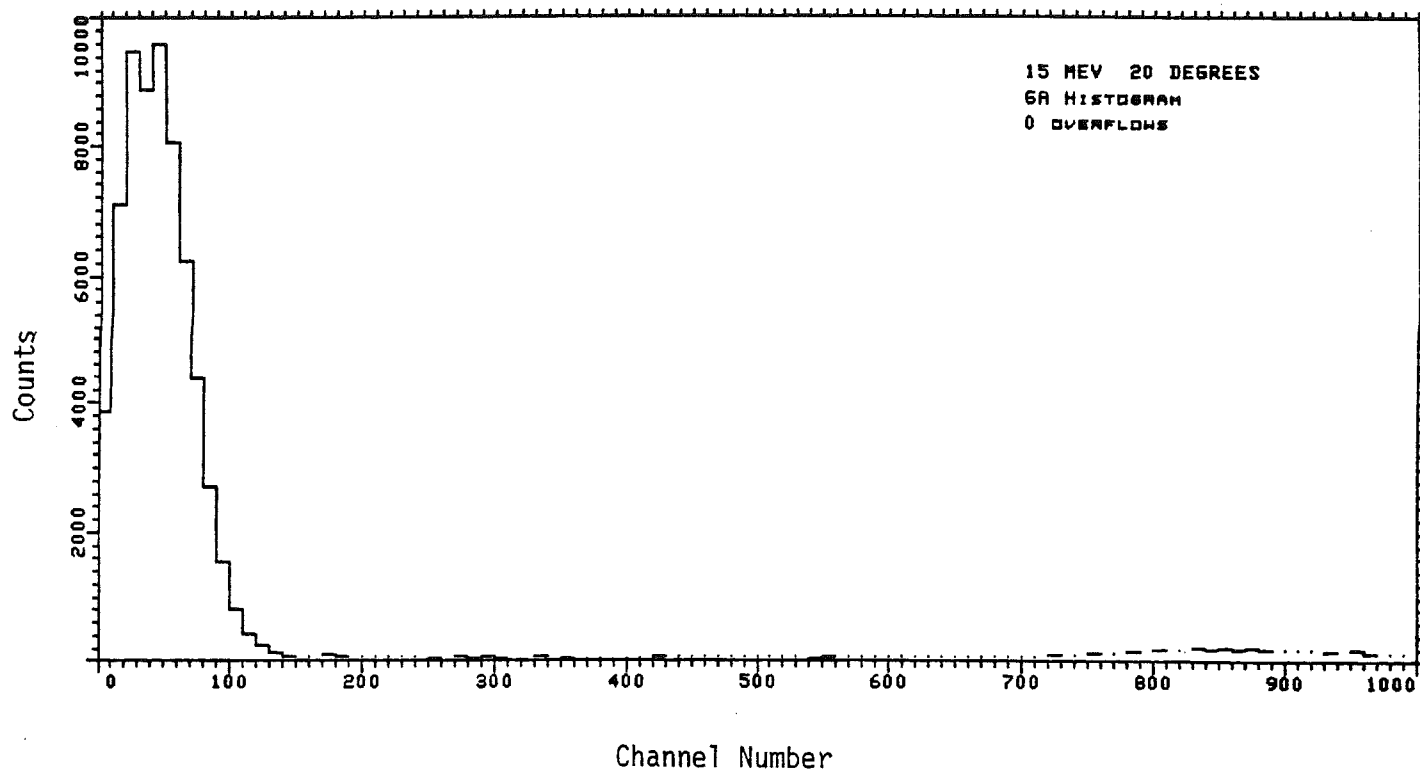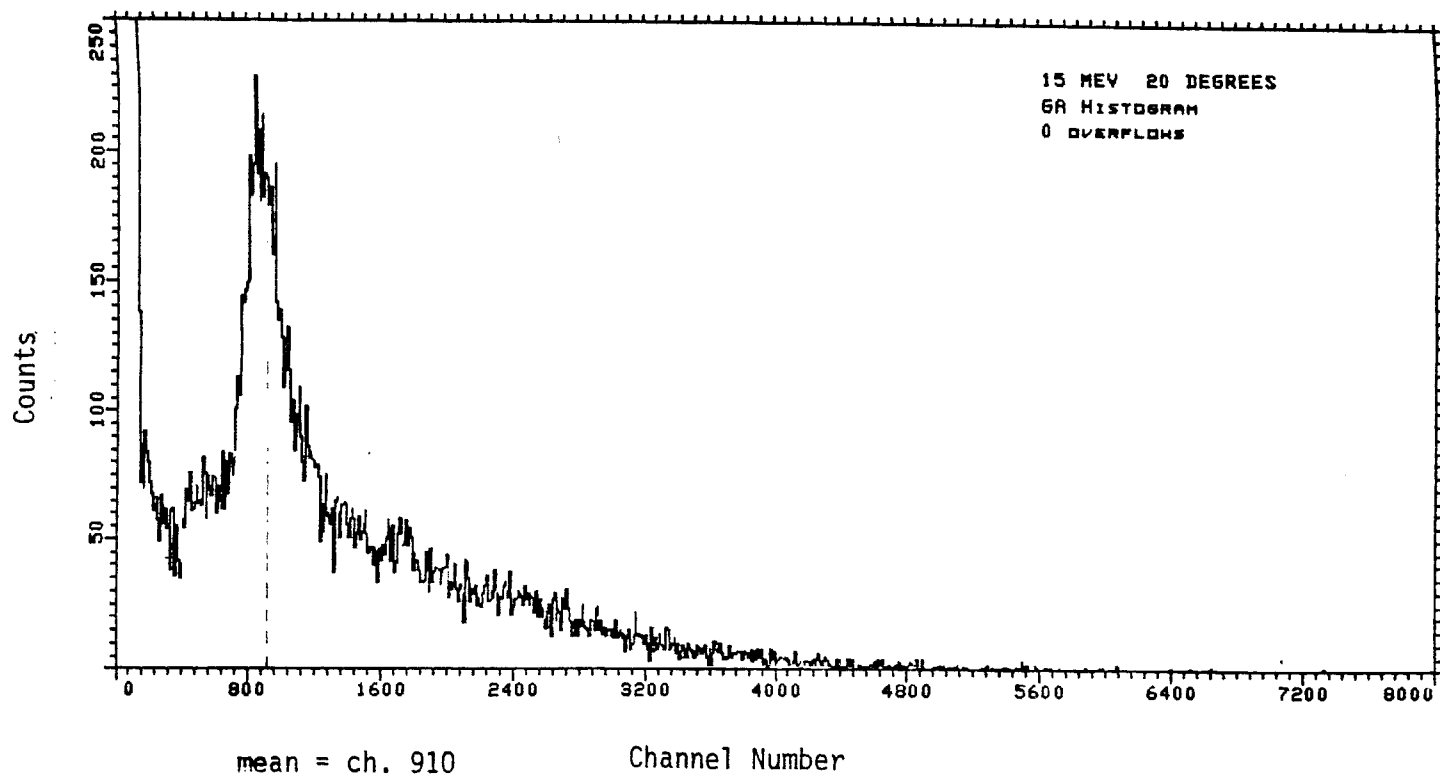
Figure 8b

28 MEV 0 DEGREES
GB Histogram

Figure 9

Channel Number

Figure 10a

mean = ch. 980   Channel Number
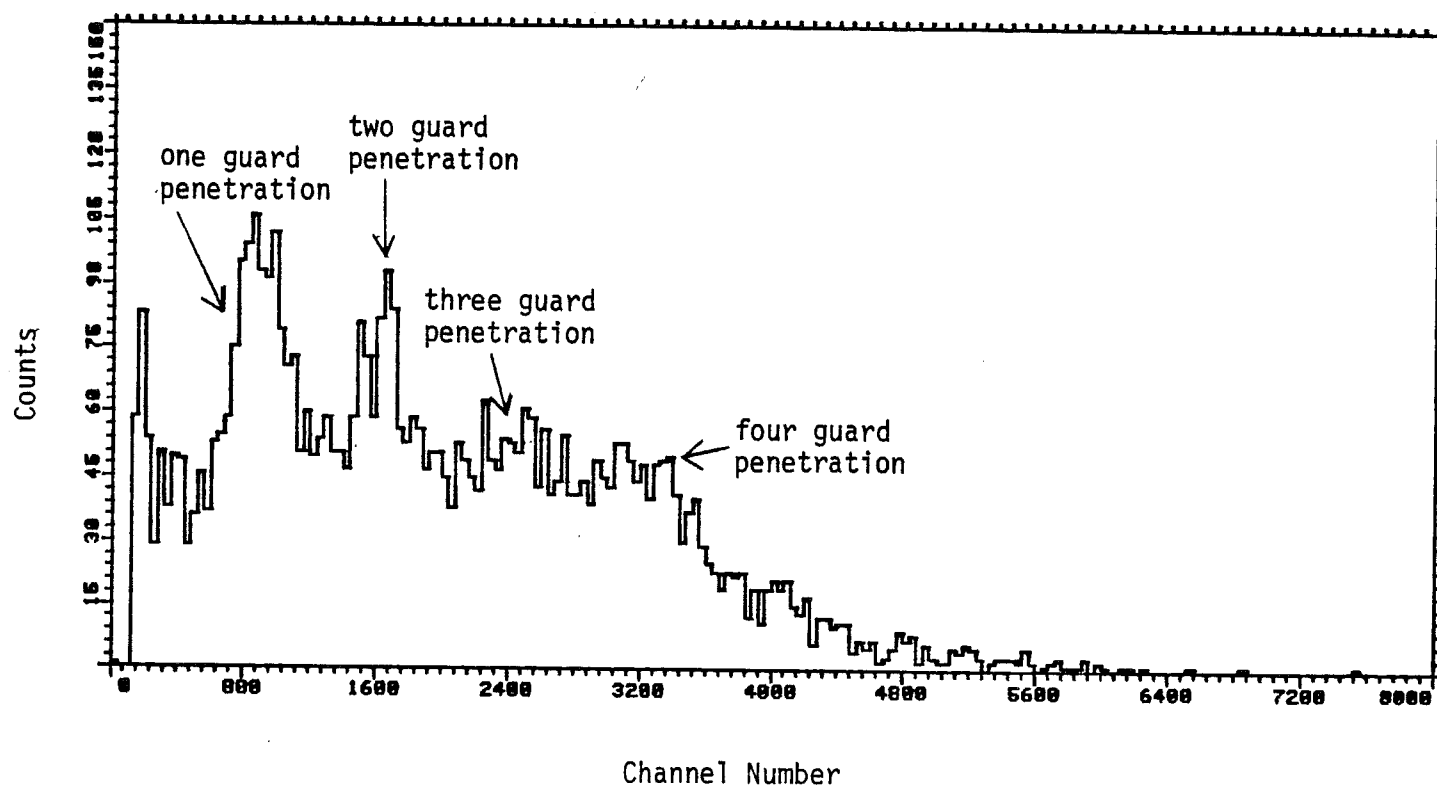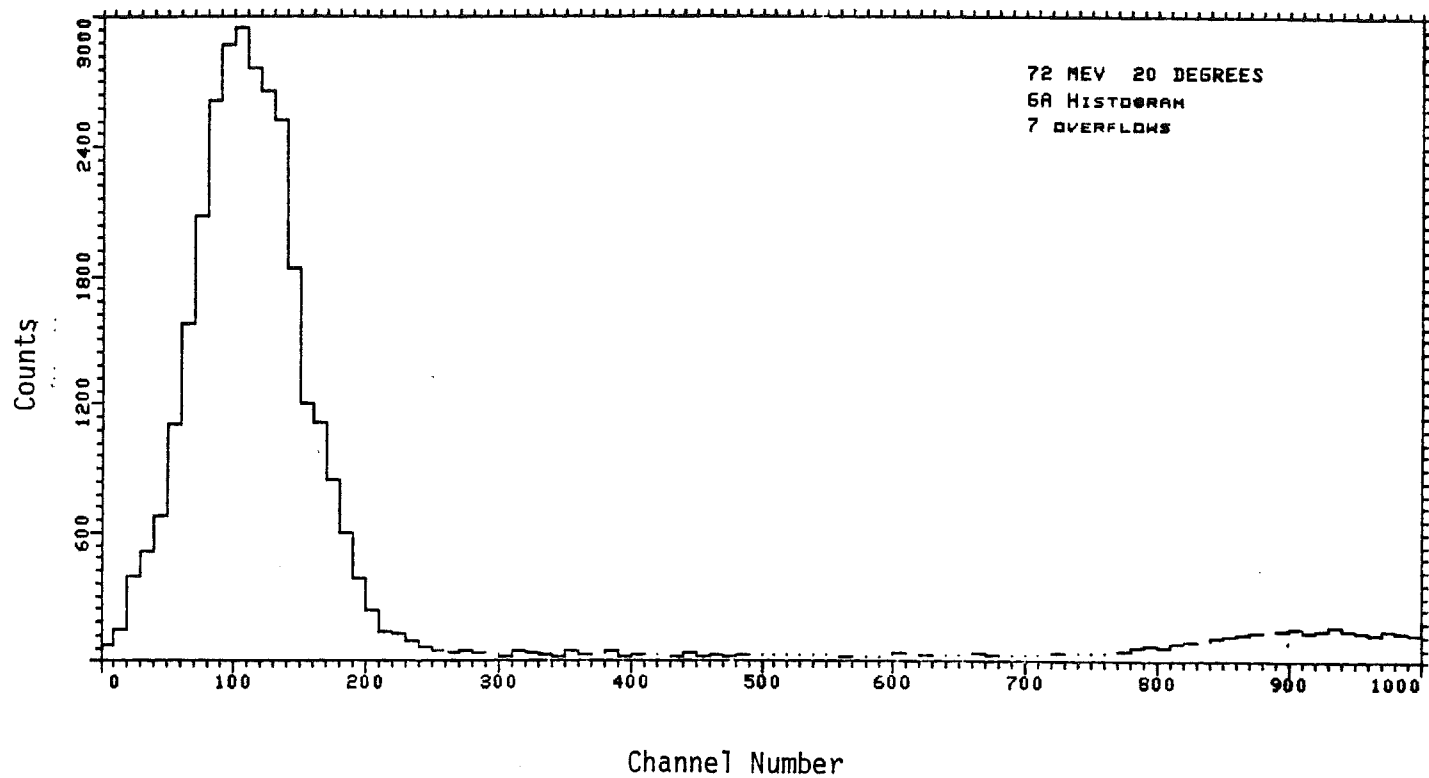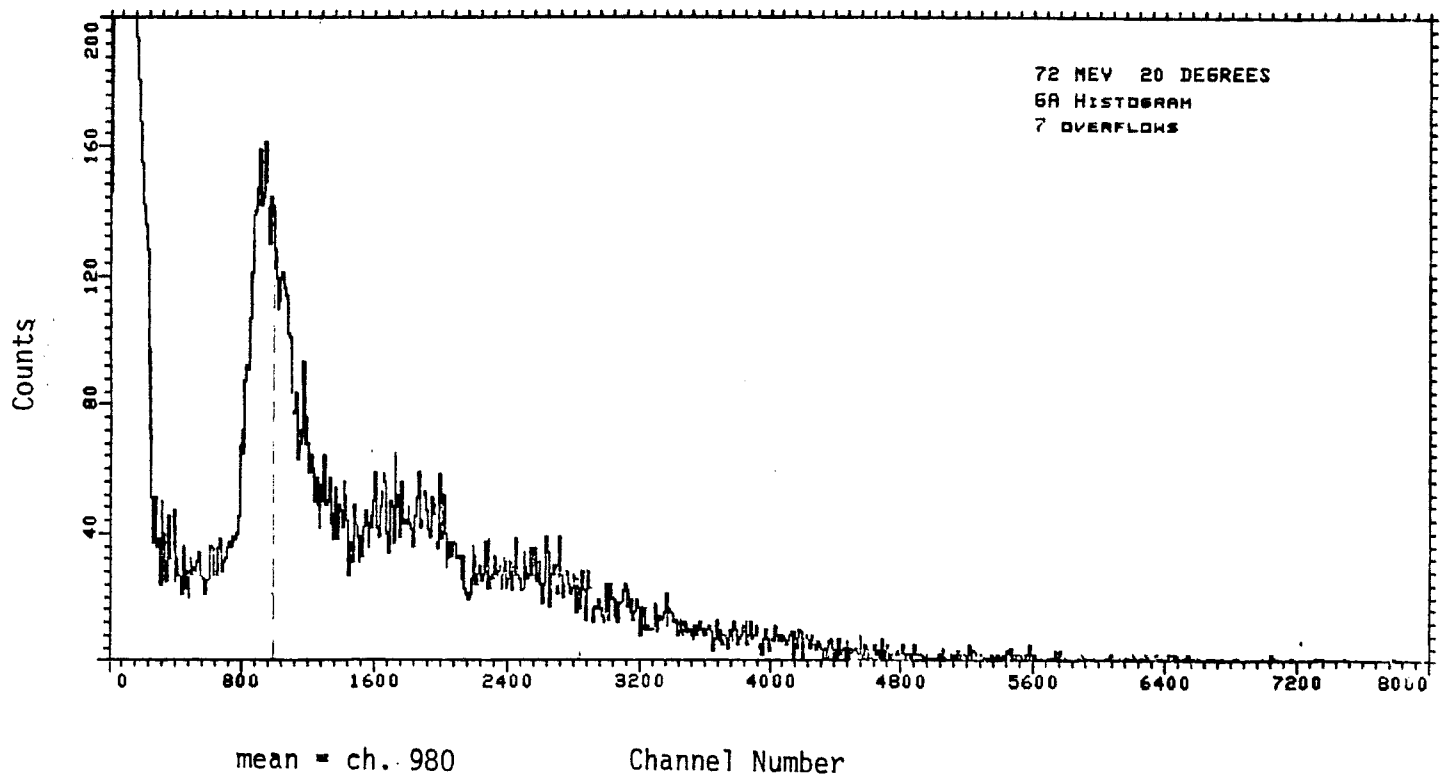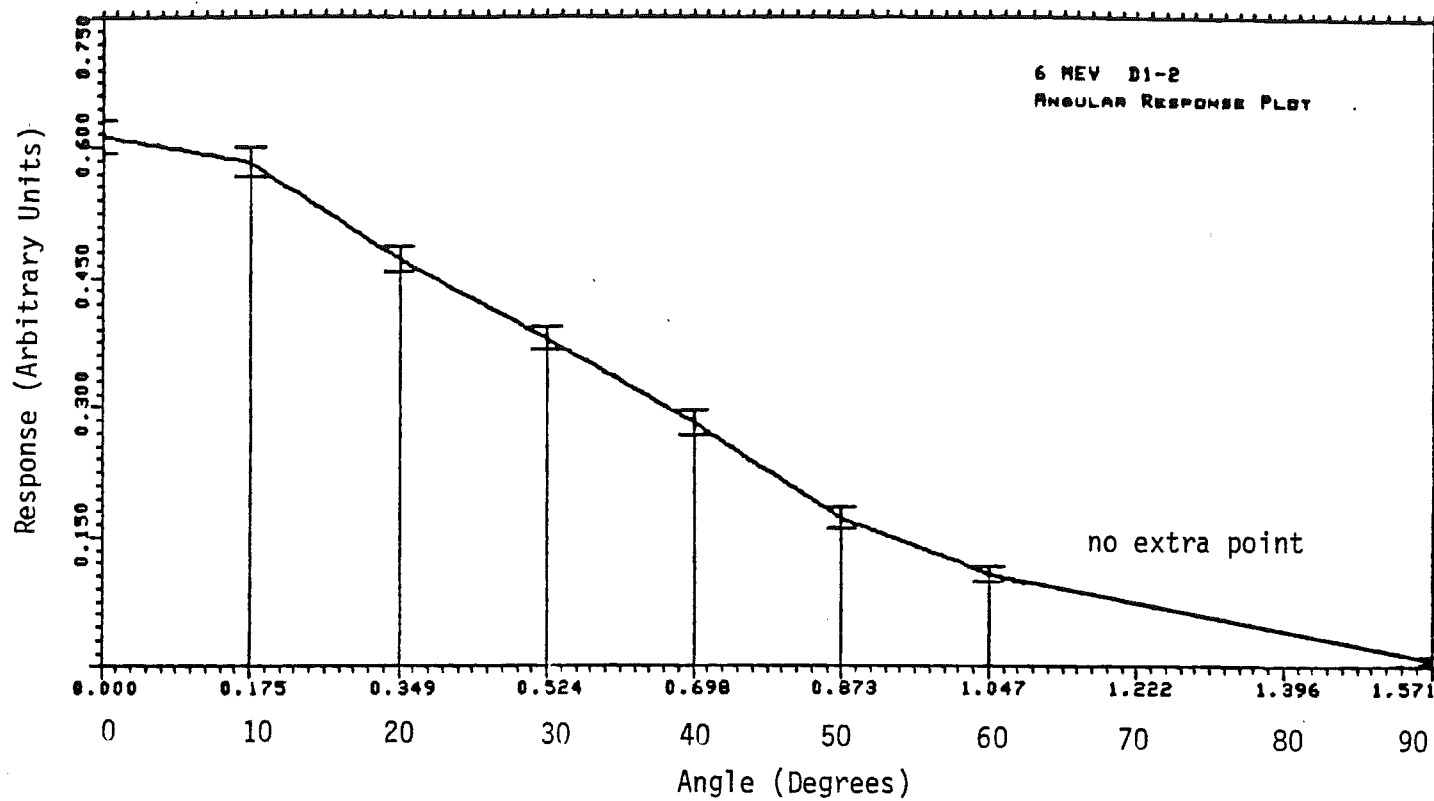
Figure 10b

Figure 11a

Figure 11b

Figure 12